INVITED PAPER *Special Issue on Measurements and Visualization Technology of Biological Information*

Fiber Tract Following in the Human Brain Using DT-MRI Data

Peter J. BASSER[†], **Sinisa PAJEVIC**[††], **Carlo PIERPAOLI**[†], *and* **Akram ALDROUBI**[†††], ***Nonmembers***

SUMMARY *In Vivo* Diffusion Tensor Magnetic Resonance Imaging (DT-MRI) can now be used to elucidate and investigate major nerve pathways in the brain. Nerve pathways are constructed by a) calculating a continuous diffusion tensor field from the discrete, noisy, measured DT-MRI data and then b) solving an equation describing the evolution of a fiber tract, in which the local direction vector of the trajectory is identified with the direction of maximum apparent diffusivity. This approach has been validated previously using synthesized, noisy DT-MRI data. Presently, it is possible to reconstruct large white matter structures in the brain, such as the corpus callosum and the pyramidal tracts. Several problems, however, still affect the method's reliability. Its accuracy degrades where the fiber-tract directional distribution is non-uniform, and background noise in diffusion weighted MRIs can cause computed trajectories to jump to different tracts. Nonetheless, this method can provide quantitative information with which to visualize and study connectivity and continuity of neural pathways in the central and peripheral nervous systems *in vivo*, and holds promise for elucidating architectural features in other fibrous tissues and ordered media.

key words: *MRI, DTI, DT, diffusion, tensor, human, brain, white matter, fiber, tract, trajectory, artifact, noise*

1. Introduction

Diffusion tensor MRI (DT-MRI) [1] is the first noninvasive *in vivo* imaging modality with the potential to generate realistic fiber-tract trajectories in soft fibrous tissues, such as nerves, muscles, ligaments, and tendons [1]–[3]. There are several technical and mathematical prerequisites, however, to achieving this important goal: First, the resolution and quality of diffusion weighted images (DWIs) *in vivo* must be sufficiently high. Second, one must provide a means to construct a continous fiber trajectory using discrete, noisy, direction field data. This entails generating a continuous, smooth representation of the discrete diffusion tensor data [4], and then developing an algorithm for following individual fiber [1], [5]–[7].

DT-MRI fiber tractography is quickly becoming a subspecialty of MRI. Several groups have proposed tractography methods, and have reported success in following fiber tracts, and even individual fascicles over distances on a gross anatomical length scale [8]–[11].

The aims of this paper are to a) describe a methodology to calculate continuous fiber-tract trajectories from discrete measured diffusion tensor MRI data, b) demonstrate that this method can follow fiber tracts in the brain using *in vivo* DT-MRI data, c) describe artifacts and inherent limitations of fiber tract following schemes that employ DT-MRI data, and d) discuss potential applications of DT-MRI fiber tractography.

2. Theory

2.1 Evolution of Fiber-Tract Trajectories

Previously, we proposed that white matter fiber-tract trajectory could be represented as a three-dimensional space curve [5]–[7] i.e., a vector, $\mathbf{r}(s)$, parameterized by the arc length, s, of the trajectory. The equation describing the evolution of $\mathbf{r}(s)$ is [12]:

$$\frac{d\mathbf{r}(s)}{ds} = \mathbf{t}(s) \tag{1}$$

where $\mathbf{t}(s)$ is the unit tangent vector to $\mathbf{r}(s)$ at s.

We also asserted that the normalized eigenvector, $\boldsymbol{\varepsilon}_1$, associated with the largest eigenvalue of the diffusion tensor, $\underline{\mathbf{D}}$, λ_1, lies parallel to the local fiber-tract direction [1], [2] in coherently organized white matter. To within acceptable experimental error, several groups have confirmed this to be true in the heart [13], [14].

A key idea in this fiber tract following algorithm is in equating the tangent vector, $\mathbf{t}(s)$, and the unit eigenvector, $\boldsymbol{\varepsilon}_1$, calculated at position $\mathbf{r}(s)$:

$$\mathbf{t}(s) = \boldsymbol{\varepsilon}_1(\mathbf{r}(s)) \tag{2}$$

Thus, combining Eq. (1) and (2) we obtain:

$$\frac{d\mathbf{r}(s)}{ds} = \boldsymbol{\varepsilon}_1(\mathbf{r}(s)) \tag{3}$$

The system of three implicit (vector) differential equations, Eqs. (2) and (3), are implicit and forced. Finally, one must specify an initial condition or starting point along the fiber tract:

$$\mathbf{r}(0) = \mathbf{r}_0 \tag{4}$$

Manuscript received October 17, 2001.

[†]The authors are with the Section on Tissue Biophysics & Biomimetics, NICHD (National Institute of Child Health & Human Development), Bethesda, MD, U.S.A.

[††]The author is with Mathematical Statistics and Computing Laboratory (MSCL), Center for Information Technology (CIT); NIH, Bethesda, MD, U.S.A.

[†††]The author is with the Department of Mathematics, Vanderbilt University, Nashville, TN, U.S.A.

3. Methods

In general, no analytical solution exists for $\mathbf{r}(s)$, so numerical methods must be employed to determine fiber-tract trajectories. Euler's method (e.g., see [15]) is didactically the best scheme to illustrate the mechanics of tract tracing. It entails starting at some point along a putative fiber, calculating the local direction of maximum diffusivity, and following that direction for a short distance. The last two steps can now be repeated starting at a new point on the trajectory. Successive iterations result in a set of discrete points along the fiber, $\mathbf{r}(s)$. Euler's method is easy to explain and to implement, but it is accurate only to 1st-order, and thus can result in large accumulated errors and eventually numerical instabilities [15]. Since our continuous representation of the diffusion tensor, $\underline{\mathbf{D}}(\mathbf{x})$ can furnish estimates of 2nd and higher-order derivatives of $\varepsilon_1(\mathbf{x})$, it is prudent to use this additional information to integrate these trajectories [16]. Thus, 2nd-order or adaptive 4th-order Runge-Kutta methods are preferred to Euler's method to solve the system of differential equations above. A 4th-order Runge-Kutta scheme described in Numerical Recipes [15], has been implemented as a callable subroutine within IDL (Research Systems, Inc., Boulder, CO, USA).

Of course, in order to apply these numerical schemes, we must be able to produce an estimate of $\varepsilon_1(\mathbf{x})$ anywhere within the imaging volume. The methodology to do this has been explained elsewhere [16], [17]. It entails first generating a continuous approximation of $\underline{\mathbf{D}}(\mathbf{x})$ everywhere within the imaging volume, and then calculating $\varepsilon_1(\mathbf{x})$ from it. Tensor field approximation entails finding a set of B-spline functions that smoothly "fits" the noisy discrete experimental tensor data in a least-squared sense (just as linear regression fits a line to a set of discrete noisy data points). A smooth representation of the fiber direction field can be obtained from this smooth, continuous tensor field.

Once having launched a fiber trajectory, we terminate the trajectory when any of the following conditions is satisfied: 1) the tract reaches the boundary of the imaging volume, 2) the tract reaches a region with low diffusion anisotropy (e.g., lattice anisotropy index < 0.1), 3) the radius of curvature of the tract is smaller than approximately two voxels, 4) the eigenvector that is the most collinear is not the same as the eigenvector associated with the largest eigenvalue. These "stop" conditions guard against producing spurious fiber tracts that are clearly artifactual.

3.1 Diffusion Tensor Field Templates

To test the fidelity and robustness of the fiber following algorithm, we previously synthesized a family of analytical 3-dimensional $\underline{\mathbf{D}}$ $(\mathbf{x})$ maps whose fiber-tract direction fields possess characteristics or patterns seen *in vivo*, or exhibit peculiar mathematical features or pathologies as described in [6], [18]. The signal-to-noise ratio (SNR) of these templates can be systematically varied to study the effect of background noise on the variability of the fiber direction field itself, and to assess the ability of the fiber tractography scheme to follow fibers faithfully.

3.2 DT-MRI Methods

Healthy volunteers were scanned using a 1.5 T GE Signa Horizon EchoSpeed equipped with a 2.2 G/cm gradient set, according to an approved NIH clinical protocol. A set of DWIs were acquired in six isotropically distributed directions, using an interleaved, spin-echo, echo-planar sequence, employing navigator echo correction, as described in [19]. DWI parameters were: FOV=22 cm, TE=78 ms, TR $>$ 5 sec with cardiac gating, voxel size=3.5 mm$\times$1.75 mm$\times$1.75 mm, data matrix=128$\times$128. The strength of diffusion weighting was measured by Trace($\underline{\mathbf{b}}$) (where $\underline{\mathbf{b}}$ is the b-matrix [20]–[23] calculated for each DWI), which was varied from approximately 0 to 1000 s/mm^2. An effective diffusion tensor, $\underline{\mathbf{D}}$, was calculated in each voxel according to [20]–[22]. Maps of useful MR parameters calculated from the diffusion tensor, such as Trace($\underline{\mathbf{D}}$), diffusion anisotropy measures (such as the Relative Anisotropy (RA), the Fractional Anisotropy (FA) [24] and the lattice index [25]), diffusion ellipsoid images, etc. [1], [2] all provide unique information to evaluate fiber tract architecture in the brain [26].

4. Results

4.1 Human Brain Data

Figure 1 shows a 3-D rendering of computed trajectories within the corpus callosum. This figure is obtained by launching trajectories from a multi-slice Region of Interest (ROI) located in the body of the corpus callosum in the proximity of the midline. We require that the lattice anisotropy index of all voxels within the ROI, greater than 0.6 to ensure that fiber tracts are launched from regions of coherently organized white matter with no partial volume contamination from Cerebrospinal fluid (CSF). Tracts are followed in both directions. The majority of fiber trajectories from the corpus callosum continue upward toward the cingular cortex. Interestingly, the cingulum can be clearly seen as a relatively thin bundle running antero-posteriorly above the corpus callosum. Considering that the ROI from which the trajectories originate does not include any portion of the cingulum, its inclusion implies that the tractography algorithm produced a connection between the callosal and cingular fibers. Whether this is an important

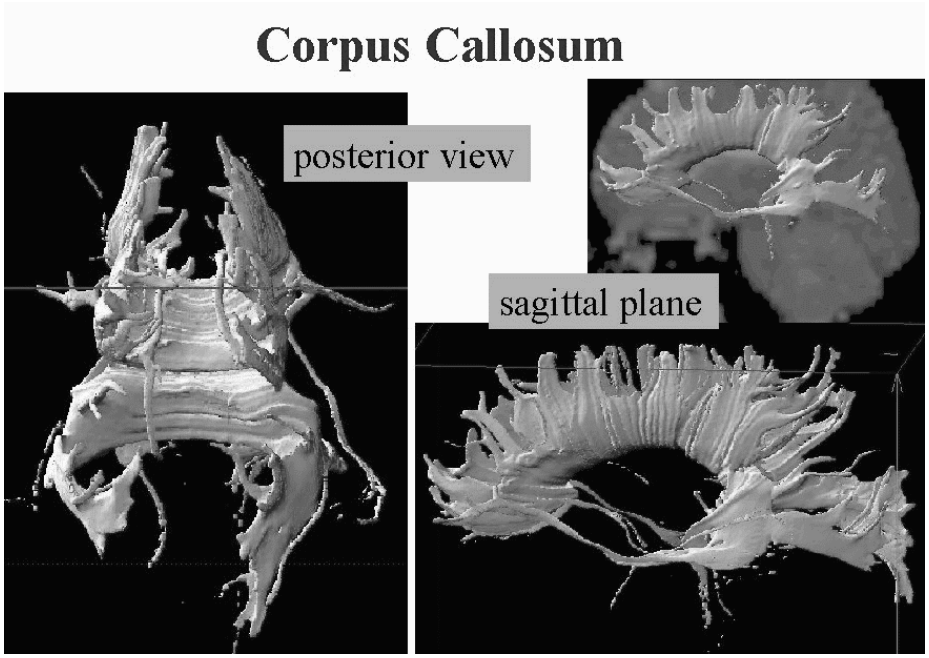

Fig. 1 Fiber-tract trajectories, $\mathbf{r}(s)$, computed from living human DT-MRI data. Trajectories were "launched" from an ROI located at the center of the splenium of the corpus callosum at its intersection with the inter-hemispheric plane. These are 3-D renderings of the computed trajectories. The figure in the upper right is juxtaposed with a T2-weighted amplitude image of the brain.

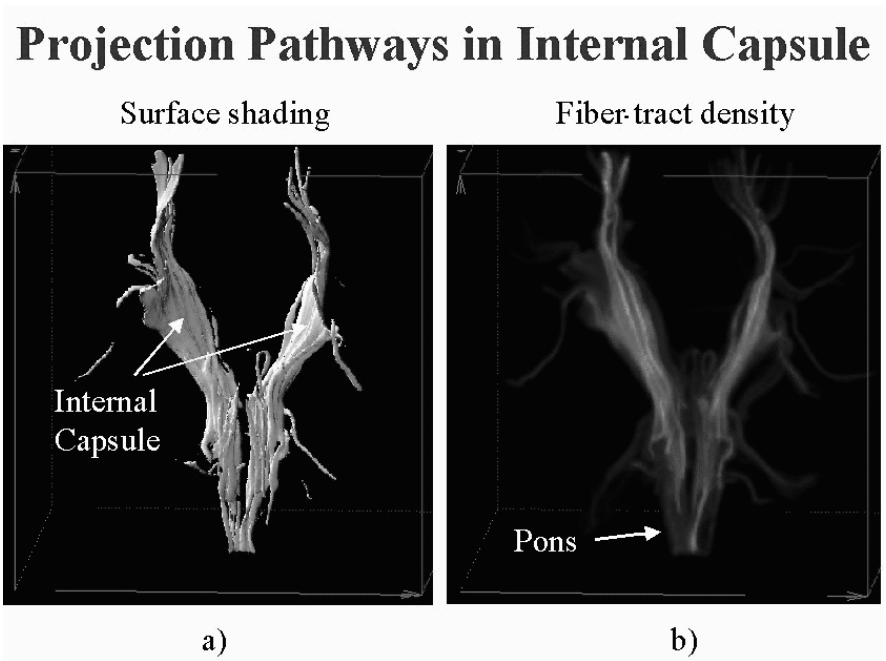

Fig. 2 3-D rendering of computed trajectories of long projection pathways from human DT-MRI data. Trajectories are launched from ROIs in the internal capsule at the level of the globus pallidum, in the pyramidal tract at the level of the cerebral peduncles and the Pons, and in the ascending sensory fibers (lemniscus medialis) at the level of the Pons. Tracts are followed in both directions. Figure 2b) shows a projection of these computed trajectories. The image intensity is proportional to the number of fibers passing through each voxel. This distribution is then projected onto the plane of view, as in a maximum intensity projection (MIP) image.

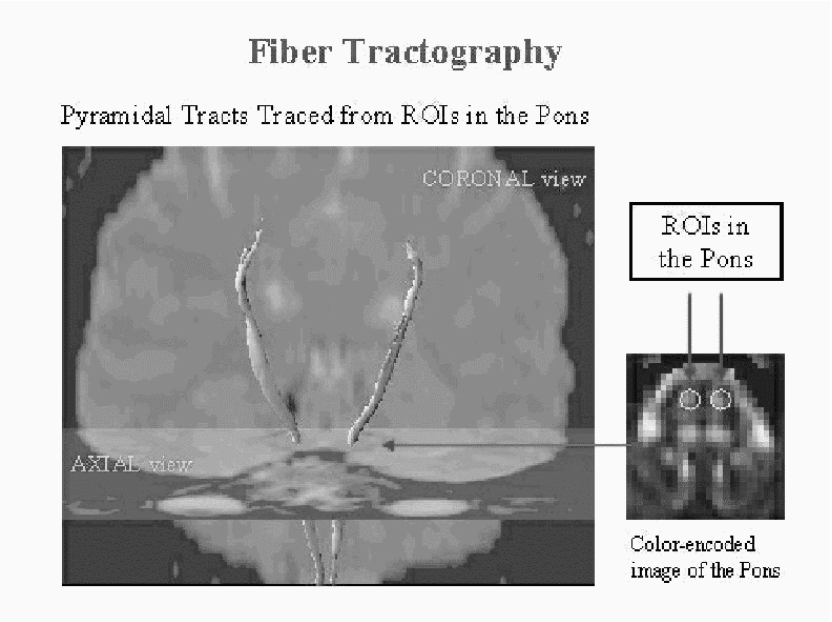

Fig. 3 A 3-D rendering of computed trajectories within the brain emanating from ROIs within the Pons containing the motor fibers. Superimposed are T2-weighted images of the brain in a coronal and axial orientation. Fibers are followed superiorly and inferiorly from the ROIs.

anatomical finding or just an artifact requires further study.

Figure 2a) also shows a 3-D rendering of computed long projection pathways human DT-MRI data. In this figure we map trajectories from ROIs positioned in the internal capsule at the level of the globus pallidum, in the pyramidal tract at the level of the cerebral peduncles and the Pons, and in the ascending sensory fibers (lemniscus medialis) at the level of the Pons. Tracts are followed in both directions. Only regions within the imaging volume for which the lattice anisotropy index is greater than 0.3 are used to ensure that fiber tracts are launched from regions of coherently organized white matter. Figure 2b) shows a projection of these computed trajectories, which is obtained from the previous figure by counting the number of fibers passing through each voxel, and assigning an intensity to each voxel which is proportional to this number. This distribution is then projected onto the plane of view, in a manner similar to the way a maximum intensity projection (MIP) image would be produced. The pathways highlighted in this figure are consistent with the known gross anatomy of the long projection pathways. Interestingly, motor fiber trajectories originating from the ROI in the cerebral peduncle usually continue superiorly up to the cortex, while sensory fiber trajectories from the ROI in the lemniscus medialis do not. This finding is consistent with the notion that sensory fibers project to the thalamus while motor fibers of the pyramidal tract descend uninterrupted from the cortex to the brainstem and the spine.

Figures 3 also shows 3-D renderings of tracts launched from an ROI within the Pons containing the Motor tracts. These fibers are followed in both directions. T2-weighted amplitude images of the brain are juxtaposed for reference.

5. Discussion

5.1 Obstacles to DT-MRI Tractography

There are several obstacles to elucidating fiber-tract trajectories quantitatively. First, there is presently no "gold standard" for *in vivo* fiber tractography [27]. In fact, DT-MRI is the only method of which we are aware that permits the calculation and visualization of fiber-tract trajectories in optically turbid tissue *in vivo* (and was developed, in part, to address this unmet need). *In vitro* validation of fiber-tract direction fields obtained by DT-MRI has been attempted histologically [13], [14]. Of course, sample registration, dissection, freezing, dehydration, fixation, microtoming, thawing, etc., each can alter tissue microstructure and microanatomy, and introduce geometric distortion in the histological sample. Therefore, great care must be used to compare fiber directions in living tissue and a fixed specimen prepared from it. Thus, the diffusion tensor field templates take on greater importance in helping us to validate fiber tracking methods that use DT-MRI data.

All of the usual artifacts and problems in DWI experiments can adversely affect fiber tracking in predictable ways. Misregistration of DWIs caused by eddy current distortion, ghosting due to motion artifacts,

and signal loss due to susceptibility variations all can affect the computed trajectories. However, many of these problems can be mitigated. The use of isotropic voxels is recommended to ensure that the accuracy of the tractography scheme is independent of fiber direction.

The diffusion tensor used to measure the fiber-tract direction is a voxel-averaged quantity. In voxels containing anisotropic fibrous tissues having a uniform fiber direction, the eigenvector associated with the largest eigenvalue of the effective diffusion tensor provides an unbiased estimate of the microscopic fiber field direction vector [28]. However, if there is a non-uniform distribution of fiber directions, the NMR signal we measure depends in a complicated way on structure and architecture of the tissue [26]. Then, the eigenvector associated with the largest eigenvalue of the effective diffusion tensor only corresponds to a consensus average fiber direction within the voxel. There, "powder averaging" of the microscopic $\underline{\mathbf{D}}$-field also occurs [25], [26]. If the voxel contains curved fiber tracts, then using smaller voxels can ameliorate this problem. If the voxel contains two or more distinct populations, for example, interdigitating distinct fiber populations, then reducing voxel size does not remedy the problem [25]. This powder averaging problem becomes even more severe where singularities in the microscopic direction field occur [6], [7], [29], [30], for example, where fiber tracts cross or "kiss," or branch or merge. Within such singular regions, fiber-tract trajectories calculated from the original or smoothed direction field may fail to follow the true fiber-tract trajectory. While recently proposed methods of Bossart et al. [31], and of Tuch et al. [32] attempt to identify two non-exchanging populations of water molecules that diffuse anisotropically within a voxel, they do not address how such fibers are *connected* within a singular region. Do they kiss, cross, or is their pattern some combination of both? A future challenge is to circumvent powder averaging effects by employing additional *a priori* anatomical information about the distribution of fiber-tract directions and structural information about tissue composition within these voxels, so one can reconstruct white matter fiber-tract trajectories in complex structures such as the ventral internal capsule, the optic chiasm, the pyramidal tract, and in other white matter structures where the fiber direction field may not be uniform.

Moreover, at points where there are discontinuities in $\mathbf{r}(s)$, or in its derivatives (such as where there are transections, or at points where the fiber tract is kinked), tractography methods that "regularize" [9] the computed fiber trajectory may be artifactually continuous there. This problem would apply particularly to schemes that introduce "memory" or which model the tract as having some inherent "bending stiffness." Generally, our ability to observe wiggles, gaps or discontinuities in fiber tracts depends upon a number of variables, such as the radius of the fiber, the width of the gap, the voxel size, the scale of the smoothing window, the background noise level, and the algorithm used. If the smoothing window is too large, it is possible to smooth over a transected fiber so it will appear continuous.

Other artifacts may be introduced when smoothing a noisy diffusion tensor field. Generating a continuous approximation to the tensor field can introduce phantom connections between tracts, which do not exist anatomically. In an attempt to make the field continuous within white matter regions, distinct fiber tracts, which may be separated from each other by a voxel or two, may be artifactually bridged or merged. In this way, "blebs" on different neighboring tracts could coalesce to form an artifactual connection or nexus, which can cause the computed trajectory to "jump" tracts. The larger the smoothing window chosen for the tensor approximation, the greater the likelihood of this problem.

Not remediating noise in the DWIs can also have adverse effects on tractography. First, it can cause one to sort eigenvectors incorrectly [18]. This can result in a sudden 90° deviation in the computed trajectory, which can cause the trajectory to "jump" to another tract [18]. Noise in DT-MRI data also introduces scatter in the distribution of the eigenvectors [3], even when the eigenvalues are sorted correctly. Also, a fiber-tracking scheme that follows noisy (interpolated) eigenvector data will eventually meander away from the true trajectory in a random fashion. Moreover, owing to noise, MRI data obtained under the same experimental conditions is not expected to produce identical trajectories. Particularly troubling is that noise-induced artifacts above can produce anatomically plausible but erroneous nerve trajectories and potentially false connections.

In our *in vivo* studies, we observed significant differences in both the geometry (i.e., shape) and *topology* (i.e., branching pattern) of fiber-tract trajectories when we perturb their starting points slightly (i.e., on a length scale smaller than an individual voxel). A direct consequence is that one could infer an altogether different "connectivity" pattern and biological function of adjacent tracts. Whether this observation is anatomically correct is not ascertainable at this time.

With the many concerns raised and *caveats* described above about fiber tractography using DT-MRI data, one should view reports of newly discovered white matter fiber pathways within the brain with healthy skepticism, as these findings could easily be due to one of the many artifacts described above. In evaluating any DT-MRI fiber tractography study, one should be convinced that all possible artifacts were considered, assessed, controlled for, and remedied.

5.2 Applications of DT-MRI Tractography

DT-MRI tractography should improve our understand-

ing of brain pathology, particularly of white matter abnormalities occurring in closed head trauma, stroke, etc.. It is also likely that DT-MR fiber tractography will be used to follow trajectories of the peripheral nervous system (PNS). There, branching patterns are simpler to follow than in the Central Nervous System (CNS), and the distances over which fiber direction and architectural organization are uniform are greater. Changes in diameter of injured nerves, and localized bulging or necking of fiber tracts might also be detectable using this approach. Radial displacement of a computed fiber tract could indicate a region of local nerve swelling or focal compression. A localized net displacement of a computed fiber tract could indicate nearby pathological tissue regions.

Finally, DT-MRI fiber tractography methods could be applied to other fibrous tissues, such as the heart, whose fiber directional pattern and organization is critical in following its normal development and diagnosing disease. Tractography adds new information to what is provided by the computed fiber direction field [33].

Methods to visualize fiber tracts that employ contrast agents, such as Manganese [34] are complementary with DT-MRI fiber tractography, and could be used in conjunction with it.

6. Concluding Remarks

Here we have reduced the difficult task of tracing the trajectory of white matter fiber tracts *in vivo* to solving a tractable system of ordinary differential equations that incorporate measured DT-MRI data.

The primary applications of DT-MRI fiber tractography are in establishing 1) whether and how different regions of the brain that perform critical processing tasks are connected via large fiber pathways [6], [18], [35] and 2) whether a white matter fiber tract is continuous [6]. The first problem entails determining whether two points (or two different ROIs) can be joined by one or more fiber-tract trajectories, which is a two-point boundary value problem. The second problem entails following a trajectory from one point along a fiber to its terminus, which is an initial-value problem.

Coherently oriented white matter tracts, such as the corpus callosum, can be followed provided that the artifacts brought to light above are carefully assessed and systematically addressed.

DT-MRI fiber-tractography can provide unique quantitative and qualitative information to aid in visualizing and in studying fiber-tract architecture in the brain and in other fibrous tissues. It has the potential to advance our understanding of connectivity and continuity in the central and peripheral nervous system *in vivo*.

References

[1] P.J. Basser, J. Mattiello, and D. Le Bihan, "MR diffusion tensor spectroscopy and imaging," Biophys. J., vol.66, no.1, pp.259–267, 1994.
[2] P.J. Basser and D. Le Bihan, "Fiber orientation mapping in an anisotropic medium with NMR diffusion spectroscopy," 11th Annual Meeting of the SMRM, Berlin, p.1221, 1992.
[3] P.J. Basser, "Quantifying errors in fiber direction and diffusion tensor field maps resulting from MR noise," 5th Scientific Meeting of the ISMRM, Vancouver, p.1740, 1997.
[4] A. Aldroubi and P.J. Basser, "Reconstruction of vector and tensor fields from sampled discrete data," in Contemporary Mathematics, ed. L.W. Baggett and D.R. Larson, pp.1–15, AMS, Providence, RI, 1999.
[5] P.J. Basser and B.J. Roth, "Stimulation of a myelinated nerve axon by electromagnetic induction," Med. Biol. Eng. Comput., vol.29, no.3, pp.261–268, 1991.
[6] P.J. Basser, "Fiber-Tractography via Diffusion Tensor MRI (DT-MRI)," 6th ISMRM, Sydney, AU. p.1226, 1998.
[7] P.J. Basser, "New histological and physiological stains derived from diffusion-tensor MR images," Ann. N.Y. Acad. Sci., vol.820, pp.123–138, 1997.
[8] D.K. Jones, A. Simmons, S.C. Williams, and M.A. Horsfield, "Non-invasive assessment of axonal fiber connectivity in the human brain via diffusion tensor MRI," Magn. Reson. Med. vol.42, no.1, pp.37–41, 1999.
[9] C. Poupon, C.A. Clark, V. Frouin, I. Bloch, D. Le Bihan, and J.-F. Mangin, "Tracking white matter fascicles with diffusion tensor imaging," 8th Annual Meeting of the ISMRM, Philadelphia, p.325, 1999.
[10] S. Mori, B.J. Crain, V.P. Chacko, and P.C. van Zijl, "Three-dimensional tracking of axonal projections in the brain by magnetic resonance imaging," Ann. Neurol., vol.45, no.2, pp.265–269, 1999.
[11] N.F. Lori, T.S. Cull, E. Akbudak, A.Z. Snyder, J.S. Shimony, H. Burton, M.E. Raichle, and T.E. Conturo, "Tracking neuronal fibers in the living human brain with diffusion MRI," ISMRM, Philadelphia, p.324, 1999.
[12] F. Frenet, Sur les courbes à doublette courbure, Toulouse, France, 1847.
[13] D.F. Scollan, A. Holmes, R. Winslow, and J. Forder, "Histological validation of myocardial microstructure obtained from diffusion tensor magnetic resonance imaging," Am. J. Physiol. vol.275(6 Pt 2), pp.H2308–H2318, 1998.
[14] E.W. Hsu, A.L. Muzikant, S.A. Matulevicius, R.C. Penland, and C.S. Henriquez, "Magnetic resonance myocardial fiber-orientation mapping with direct histological correlation," Am. J. Physiol. vol.274(5 Pt 2), pp.H1627–H1634, 1998.
[15] W.H. Press, S.A. Teukolsky, W.T. Vetterling, and B.P. Flannery, Numerical Recipes in C, Cambridge University Press, Cambridge, 1992.
[16] S. Pajevic, P.J. Basser, and A. Aldroubi, "A continuous tensor field approximation for DT-MRI data," ISMRM, Glasgow, p.1535, 2001.
[17] S. Pajevic, A. Aldroubi, J. Duda, and P.J. Basser, "A continuous tensor field approximation of discrete DT-MRI data for extracting microstructural and architectural features of tissues," J. Magn. Reson., 2001.
[18] P.J. Basser, S. Pajevic, C. Pierpaoli, J. Duda, and A. Aldroubi, "In vivo fiber-tractography in human brain using diffusion tensor MRI (DT-MRI) data," Magn. Reson. Med. vol.44, no.4, pp.625–632, 2000.
[19] A. Virta, A. Barnett, and C. Pierpaoli. Visualizing and characterizing white matter fiber structure and architecture

in the human pyramidal tract using diffusion tensor MRI. Magn Reson Imaging, vol.17, no.8, pp.1121–1133, 1999.

[20] P.J. Basser, J. Mattiello, and D. Le Bihan, "Estimation of the effective self-diffusion tensor from the NMR spin echo," J. Magn. Reson. vol.B 103, no.3, pp.247–254, 1994.

[21] J. Mattiello, P.J. Basser, and D. Le Bihan, "The b matrix in diffusion tensor echo-planar imaging," Magn. Reson. Med. vol.37, no.2, pp.292–300, 1997.

[22] J. Mattiello, P.J. Basser, and D. Le Bihan, "Analytical calculation of the b matrix in diffusion imaging," in Diffusion and Perfusion Magnetic Resonance Imaging, ed. D.L. Bihan, pp.77–90, Raven Press, New York, 1995.

[23] J. Mattiello, P.J. Basser, and D.L. Bihan, "Analytical expression for the b matrix in NMR diffusion imaging and spectroscopy," J. Magn. Reson., vol.A 108, pp.131–141, 1994.

[24] P.J. Basser and C. Pierpaoli, "Microstructural and physiological features of tissues elucidated by quantitative-diffusion-tensor MRI," J. Magn. Reson., vol.B 111, no.3, pp.209–219, 1996.

[25] C. Pierpaoli and P.J. Basser, "Toward a quantitative assessment of diffusion anisotropy" [published erratum appears in Magn. Reson. Med. 1997 June vol.37, no.6, p.972]. Magn. Reson. Med., vol.36, no.6, pp.893–906, 1996.

[26] C. Pierpaoli, P. Jezzard, P.J. Basser, A. Barnett, and G. Di Chiro, "Diffusion tensor MR imaging of the human brain," Radiology, vol.201, no.3, pp.637–648, 1996.

[27] F. Crick and E. Jones, "Backwardness of human neuroanatomy," Nature, vol.361, no.6408, pp.109–110, 1993.

[28] S. Pajevic and P.J. Basser, "Non-parametric statistical analysis of diffusion tensor MRI data using the bootstrap method," 8th Annual Meeting of the ISMRM, Philadelphia, p.1790, 1999.

[29] C. Pierpaoli, A.S. Barnett, S. Pajevic, A. Virta, and P.J. Basser, "Validation of DT-MRI tractography in the descending motor pathways of human subjects," ISMRM, Glasgow, p.501, 2001.

[30] C. Pierpaoli, A. Barnett, A. Virta, L. Penix, and R. Chen, "Diffusion MRI of wallerian degeneration. A new tool to investigate neural connectivity in vivo?," 6th ISMRM, Sydney, p.1247, 1998.

[31] E.L. Bossart, B.A. Inglis, D.L. Buckley, E.D. Wirth III, and T.H. Mareci, "Multiple component diffusion tensor imaging in excised fixed CNS tissue," ISMRM, Philadelphia, p.328, 1999.

[32] D.S. Tuch, R.M. Weiskoff, J.W. Belliveau, and V.J. Wedeen, "High angular resolution diffusion imaging of the human brain," ISMRM, Philadelphia, p.321, 1999.

[33] L. Garrido, V.J. Wedeen, K.K. Kwong, U.M. Spencer, and H.L. Kantor, "Anisotropy of water diffusion in the myocardium of the rat," Circ. Res., vol.74, no.5, pp.789–793, 1994.

[34] R.G. Pautler, A.C. Silva, and A.P. Koretsky, "In vivo neuronal tract tracing using manganese-enhanced magnetic resonance imaging," Magn. Reson. Med. vol.40, no.5, pp.740–748, 1998.

[35] P.J. Basser, S. Pajevic, C. Pierpaoli, J. Duda, and A. Aldroubi, "Fiber-tractography in human brain using diffusion tensor MRI (DT-MRI)," 8th Annual ISMRM, Denver, p.784, 2000.

Peter J. Basser received his A.B. degree in Engineering Sciences from Harvard College in 1980, and received both S.M. and Ph.D. degrees in Engineering Mechanics from Harvard University in 1982 and 1986, respectively. Since then, he has worked at the National Institutes of Health (NIH) in several capacities, most recently as a Senior Investigator and Chief of the Section on Tissue Biophysics and Biomimetics within the National Institutes of Child Health and Human Development (NICHD).

Sinisa Pajevic

Carlo Pierpaoli

Akram Aldroubi

Their biographies and photographs are not available.